AD 291 491

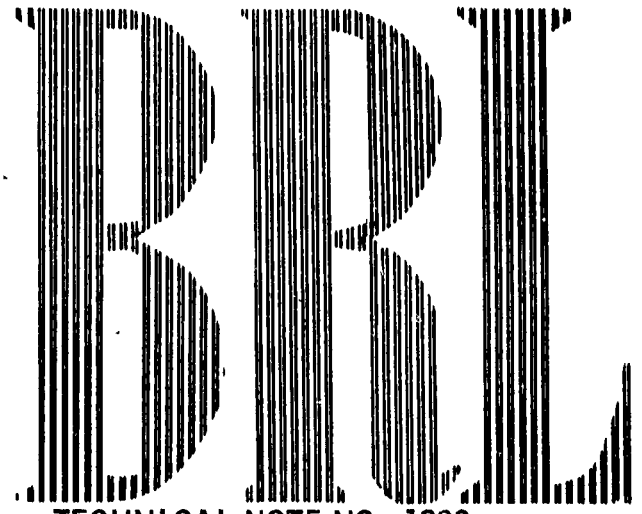

TECHNICAL NOTE NO. 1380
FEBRUARY 1961

HYPERVELOCITY MICRO-PARTICLE IMPACT ON THIN FOILS

L. G. Richards
J. W. Gehring, Jr.

Department of the Army Project No. 503-04-011
Ordnance Management Structure Code No. 5010.11.833

BALLISTIC RESEARCH LABORATORIES
ABERDEEN PROVING GROUND, MARYLAND

Destroy when no longer needed. DO NOT RETURN

B A L L I S T I C R E S E A R C H L A B O R A T O R I E S

TECHNICAL NOTE NO. 1380

FEBRUARY 1961

HYPERVELOCITY MICRO-PARTICLE IMPACT ON THIN FOILS

L. G. Richards
J. W. Gehring, Jr.

Terminal Ballistics Laboratory

Department of the Army Project No. 503-04-011
Ordnance Management Structure Code No. 5010.11.833

A B E R D E E N P R O V I N G G R O U N D, M A R Y L A N D

TABLE OF CONTENTS

B A L L I S T I C R E S E A R C H L A B O R A T O R I E S

TECHNICAL NOTE NO. 1380

LGRichards/JWGehring,Jr./sec
Aberdeen Proving Ground, Md.
February 1961

HYPERVELOCITY MICRO-PARTICLE IMPACT ON THIN FOILS

ABSTRACT

Micrometeorite bombardment of thin foils was simulated by a ballistic method of projecting cast iron particles less than 100 microns in size to 12 Km/sec. The Mylar and Testlar target foils tested were prospective balloon satellite materials. Bare and metal coated specimens, 0.5 and 2 mils thick, were included. Perforations were analysed by a photographic enlargement technique particularly adapted for complete survey of exposed target area without gaps or duplications. Statistical distributions of perforation diameters were obtained and matched with a similar distribution of the impacting fragments. Thus, the integrated impact intensity sustained by a particular target was determined. Results are reported in tabular form suitable for evaluation of changes in physical properties of the foils due to meteorite impact. These experimental methods are suitable for studies of impacts on simple metal foils.

LIST OF ILLUSTRATIONS

I. INTRODUCTION

The Ballistic Research Laboratories have been conducting a long range experimental investigation into the fundamental mechanism of target penetration and crater formation caused by impact of hypervelocity pellets.[1-3] Concurrently, the impact of pellets on thin targets is being studies to determine the penetration, perforation and spall formation characteristics, the energy of spalled particles, and the behavior of spaced and laminated targets. Both these programs, treating impacts into either finite or semi-infinite targets, are being conducted using macro pellets, 0.1 to 10.0 grams in mass and micro-pellets, 10^{-4} to 10^{-8} grams in mass with impact velocities up to 21.0 kilometers per sec.

While much of the data obtained for semi-infinite target cases has been reported in the references cited, very little has been reported on the behavior of thin targets. And, more apropos to this report, nothing has been reported on the behavior of thin foils subjected to micro-particle impact. Although data should be forthcoming from the more detailed studies of thin foils, some knowledge was urgently needed on the reaction of an inflatable balloon or balloon satellite to an impacting meteorite. (See, for instance, Reference 4). Since this target presented a unique case of a metal-plastic laminated foil, it was decided to conduct a brief program to examine these specific targets as part of the precursory study of thin target impact. The results to be reported herein cover the firing of micro-particles into Mylar and Testlar foils, each in two thicknesses, 0.0005" and 0.002"; and each in one of three conditions, uncoated, coated with steel, and coated with aluminum.

The target specimens are code-designated for ready reference of those who wish to test these materials to determine the changes in critical properties induced by hypervelocity impact. Among such properties, reduction in tensile strength and reflectivity would be important. Reference 4 indicates the importance of such mechanical tests of inflatable structure materials. The targets used in these test were furnished by the General Electric Co.

II. EXPERIMENTAL PROCEDURE

A. Description of Test Facility:

The techniques used to project micro-particles to velocities in excess of 10 Km/sec have been generally described in References 1-2, and are described in more detail in Reference 3. Slight variations of those procedures were used in these tests. In brief, small cylinders of brittle cast iron are cast into specially designed explosive charges. (See Item D, Figure 1) A charge, when fired, ejects a cluster of iron particles, all of which are less than 100 microns in size, traveling at a velocity in excess of 12 Km/sec. The velocity of this cluster of particles has been measured both optically and by flash radiography. In addition, an explosive-driven shuttering device (Reference 3) was used to establish the lower limit of particle velocity. (See Items P and S in Figure 1) This device consists of an aluminum tube aligned in the path of the particles, with the detonation of the explosive timed to close the tube so that all particles traveling at less than some desired velocity (for these tests 12 Km/sec) will be cut off. The charge setup, vacuum chambers, baffles, cutoff tube, and target mount are shown in Figure 1.

The specimen foils (T, Figure 1) were placed over one end of a 2-1/2" diameter steel tube (N, Figure 1) and held in place by another tube 3" in diameter (M, Figure 1) on the principle of the embroidery hoop. These are shown in detail in Figure 2. A polished copper plate (L, Figure 1) perforated for vacuum relief, with a spacer ring (K, Figure 1) to prevent direct contact, was used behind the foil specimen as a witness plate. A metal ring (J, Figure 1) fitted to the outer tube protects the folded edges of the specimen. Thus, an area about 2-1/4" in diameter, centrally located in the specimen gage length, was exposed to impact testing.

B. Particle Size Determination:

Since it is not possible to project individual micro-particles at these velocities, it is necessary to project a cluster of particles and to subsequently determine the mass of any one discrete particle. It has been

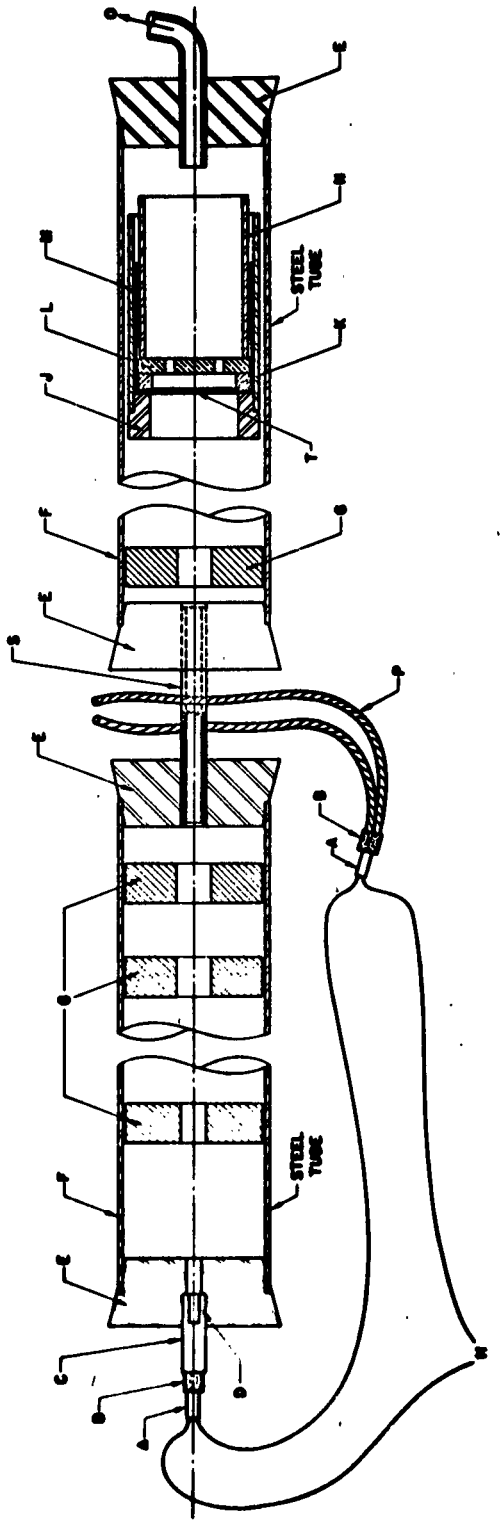

FIG. 1 - SKETCH OF ARRANGEMENT OF VACUUM CHAMBER

FIG. 2 - TARGET MOUNT FOR THIN FOIL TARGETS

TOP PHOTO: PARTIALLY ASSEMBLED WITH UNCOATED MYLAR TARGET SPECIMEN

BOTTOM PHOTO: DISASSEMBLED WITH ALUMINUM COATED TESTLAR TARGET SPECIMEN

shown[3] that the metallurgical history of the cast iron used in the cylindrical liner determines the size distribution of the particles projected from the charge. Since this size distribution is reproducible, it is therefore possible to measure and statistically determine the particle size vs. number of particles as shown in Figure 3. This distribution was determined by firing the particles into paraffin, retrieving them with a magnet, and then measuring their size and determining the frequency distribution of particle sizes. These particles are random fragments of the cast iron liner and, though roughly equiaxed, they are not truly spherical in shape. Reference 3 demonstrated that the average of the principal dimensions could be treated as equivalent to the diameter of a sphere. However, the frequency maxima and minima so determined, while definite, are not particularly sharp. Hypervelocity craters, and thin target perforations on the other hand are definitely circular and possess distinct diameters.

Since the size of a crater is proportional to the size of the impacting particle, this size distribution is also reflected in the target impacts. By carefully measuring the craters in a target, and their total number, it is possible to match the size distribution of particles to the size distribution of craters and therefore determine the size of the particle which caused a given crater in the target. Because of the definite diameter associated with a circular crater or perforation, the frequency maxima and minima in an impact diameter plot exhibit a sharpness which is masked in the corresponding particle size plot. For example, using 5-micron summation increments, particle measurement would give a frequency minimum at about 40 microns. But some 40-micron observations might be recorded where the irregular particles exhibited a dimension projected to give this measurement. Also, at least a few 38-micron to 42-micron particles would be assigned to this increment. On the other hand, in measuring the impact diameters, a value corresponding to a 40μ particle is practically never found.

This type of analysis, matching frequency distributions of particle and crater sizes, was successfully used in the study of semi-infinite metal targets (See Reference 3), and it is the procedure used to determine the

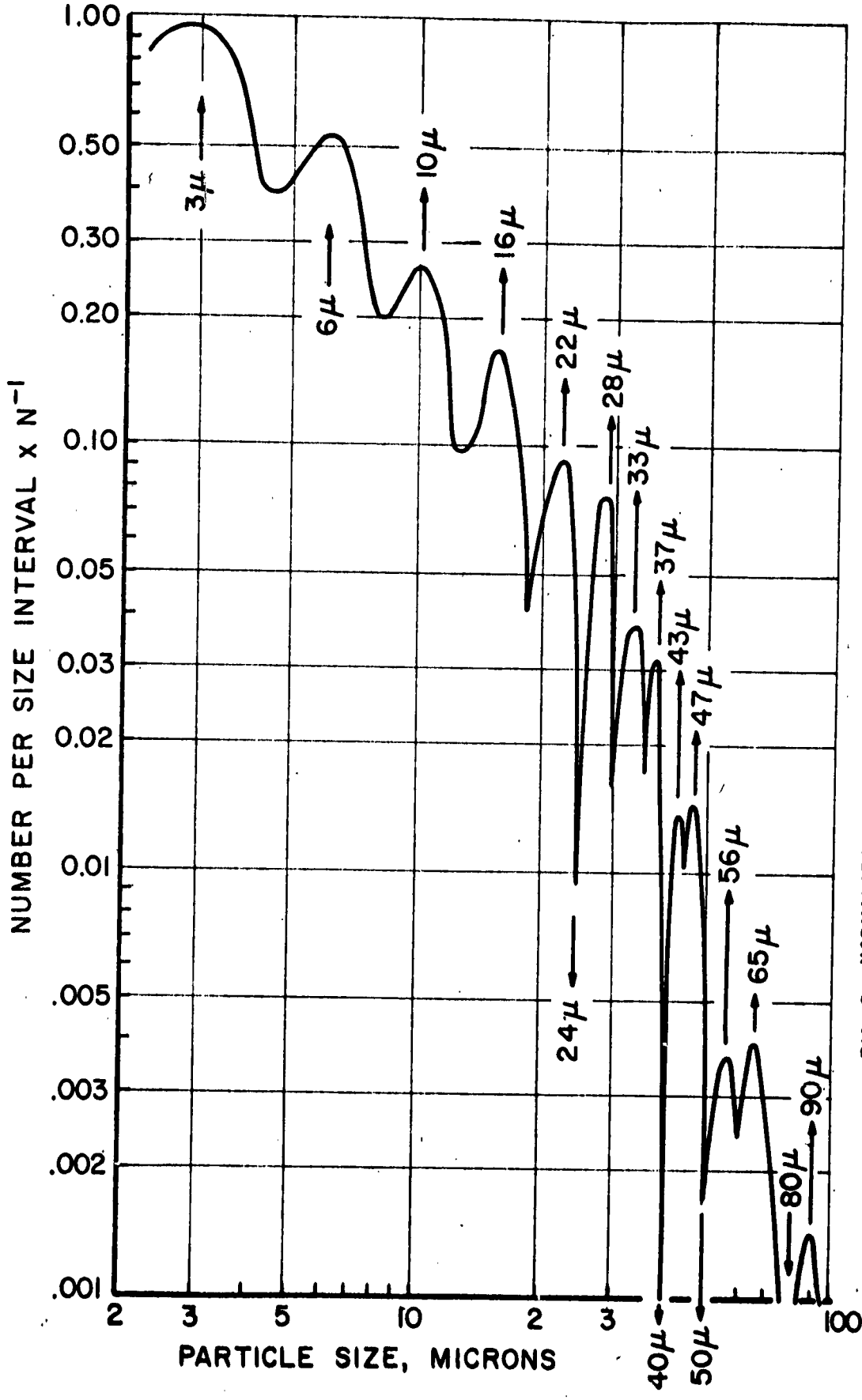

FIG. 3 - NORMALIZED SIZE DISTRIBUTION OF CAST IRON MICRO PARTICLES PROJECTED BY CYLINDRICAL LINER CHARGE.

FIG. 4 - PHOTOGRAPHIC ENLARGEMENT OF IMPACTED 2 MIL UNCOATED MYLAR TARGET. WHITE MARK IS ORIENTATION REFERENCE.

size of particle which caused a given crater or perforation in the plastic film targets of these tests. Figure 5 of Reference 3 indicates however, that the particle size distribution resulting from recovery, measurement, and counting of particle clusters projected from the cast iron liner charges needed improved detail in the range of particle size below 40 microns. Utilizing the proportionality of crater diameter to responsible particle demonstrated in Reference 3, the crater size distributions of several targets having many thousand measureable craters each have been scaled back, superimposed, and a curve drawn. This curve is shown in Figure 3.

C. Target Analysis:

A photographic enlargement method was introduced for the foil target analysis in place of the crater measurement technique described in Reference 3. This method provided several advantages over the microscopic analysis. All the difficulties of scanning a large area in small increments without gaps or overlaps are eliminated, a permanent photographic record is available for rechecking observations, and finally, the foil specimen itself is freed from long periods of exposure to possible damage in handling.

This photographic technique consists of sandwiching the specimen foil between clear glass sheets and introducing the tested area into the field of an ordinary photographic enlarger. A convenient enlargement ratio was chosen to permit recording the impacted regions on one or two sheets of 8" x 10" Ansco Reprolith Ortho or equivalent film, and the enlarger was then carefully focused to optimum sharpness. Figure 4 is a paper print taken in this manner of an uncoated 2-mil Mylar specimen. Note that a region of disturbed material shows as an opaque ring around each of the perforations. Where impact by very small particles has been particularly dense, the opaque spots merge into a cloudy area of reduced transparency. Figure 5 similarly represents an aluminum coated 2-mil Testlar target. In this target the metallic coating renders the whole background opaque. Distinct spots represent perforations of the foil. Some of the smaller less clear spots were caused by small particles penetrating only the

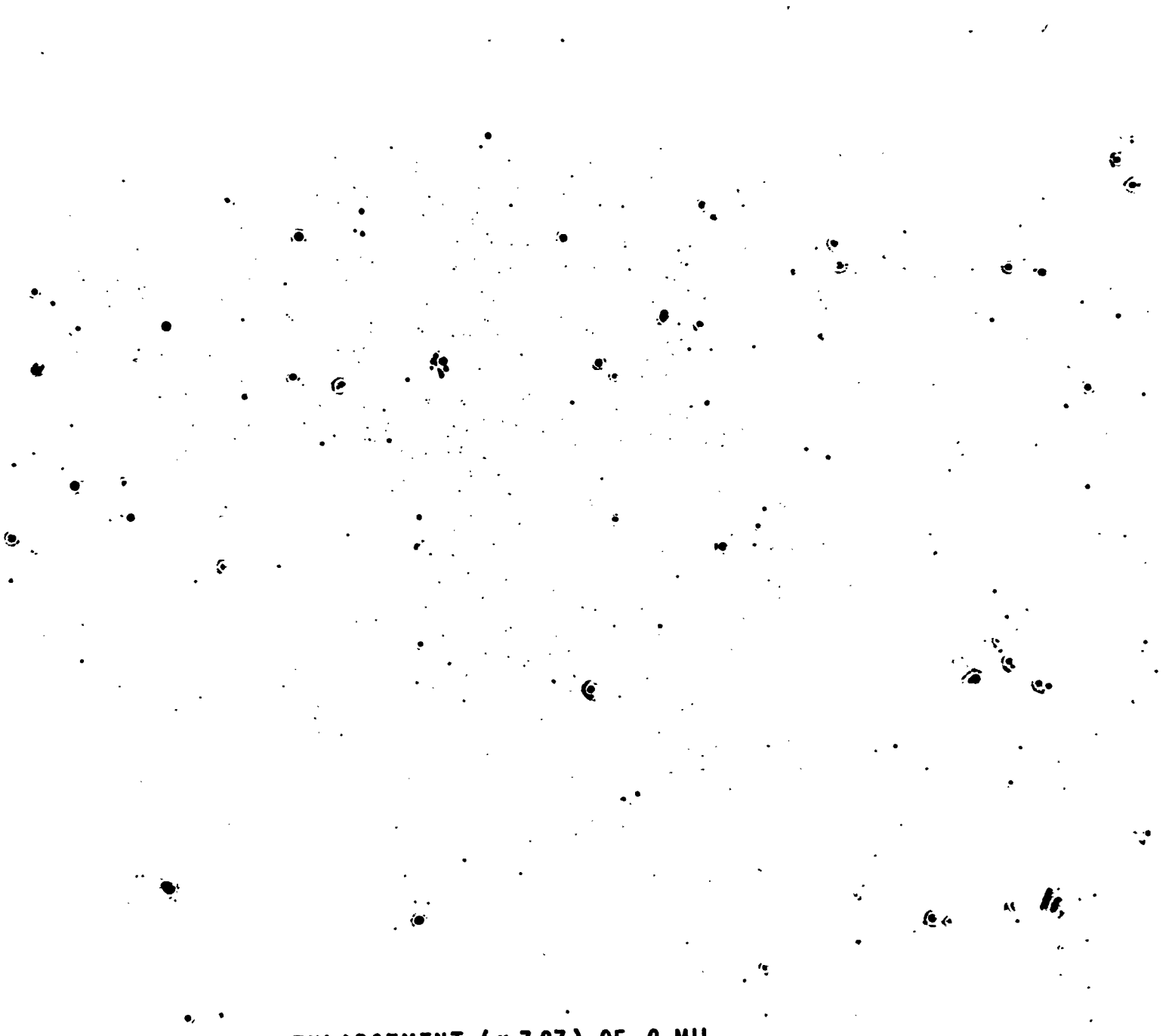

FIG. 5 PHOTOGRAPHIC ENLARGEMENT (x 7.27) OF 2 MIL ALUMINUM COATED TESTLAR TARGET

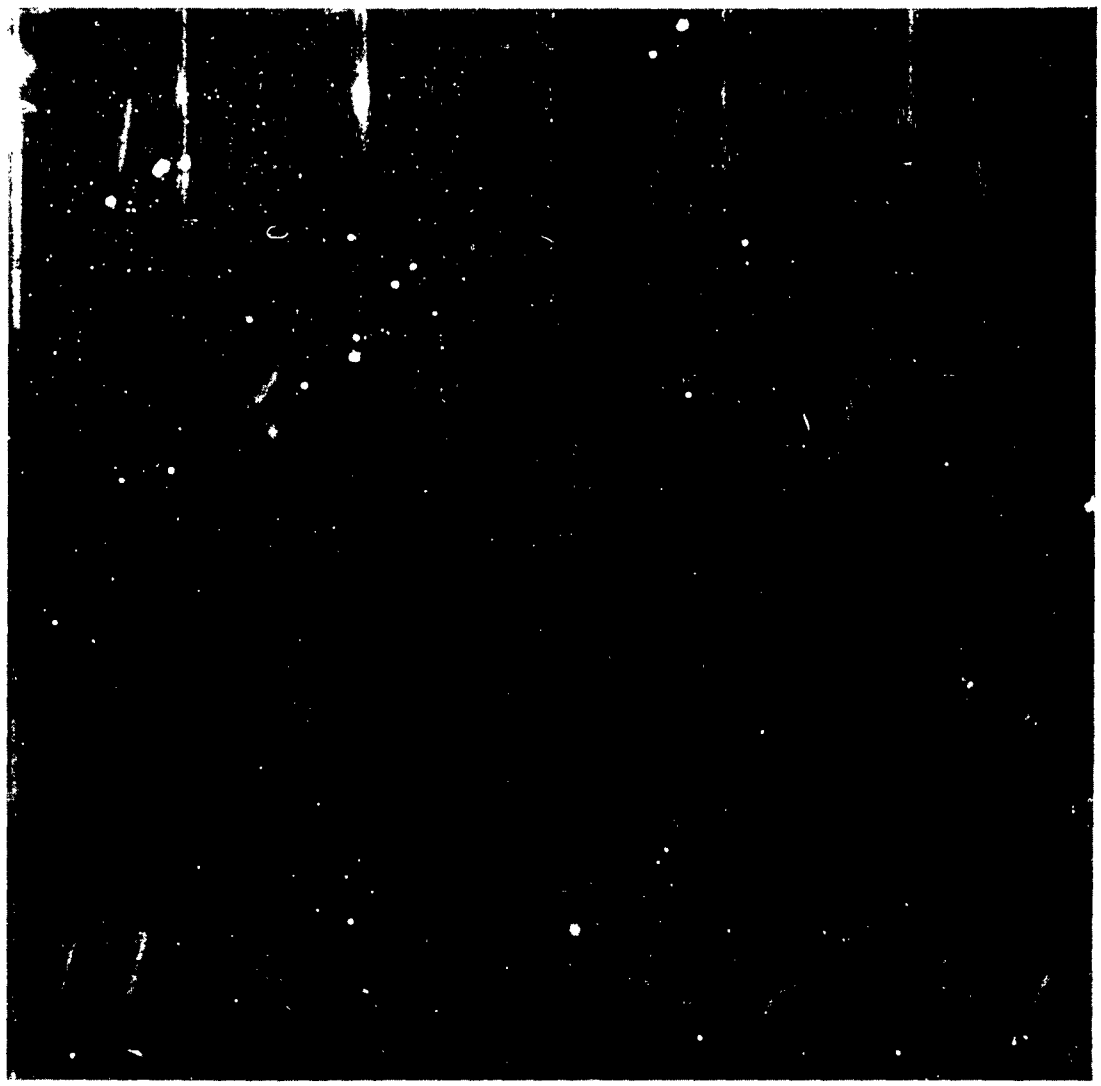

FIG. 6 CONTACT PRINT OF FIRST ENLARGEMENT FILM MOUNTED IN GLASS PLATES AND SUBDIVIDED INTO REFERENCE RECTANGLES FOR SECOND ENLARGEMENT

metallic coating. Disturbed material, either surrounding the perforations or in clouds of very small impacts, does not show. Some of the larger perforations exhibit a more or less complete circle of disturbance in the metallic coating. The significance of these indications will be discussed later. A transparent millimeter scale was enlarged with the same setting as a permanent record of the actual magnification.

When developed, this first enlargement film was similarly sandwiched between glass for re-enlarging. The field was divided into numbered reference rectangles in grease pencil on the glass. These rectangles, about 1 x 1-3/8" on the intermediate film, were then enlarged to nearly fill a sheet of 11" x 14" enlarging paper. Figure 6 shows a contact print of such a sub-divided film. Figure 7 shows a portion of one such section doubly enlarged. Note that the impact perforation profiles are relatively sharp, so that they can be clearly distinguished in spite of the grease pencil number, which is out of focus due to the thickness of the glass. Periodically, the actual magnification was permanently recorded by the introduction of the scale film, also glass-sandwich mounted, taken as a check on the original, intermediate specimen enlargement. The magnifications of these check prints vary by less than $\pm$ 1% from the average, due to minor focusing adjustments to obtain clarity and sharpness of the perforation images.

Optical parallax errors would tend to be minimized in the double enlargement technique by partial cancellation as the sense would be reversed in the second step from that in the first, negative step. However, check measurements were made of several perforations identified by using the intermediate enlargement films as a guide on a McPherson Film Comparator and on a Bausch and Lomb Contour Measuring Projector. All three methods checked within the 5-micron increments used for statistical summation.

D. Perforation Size:

Figure 8 shows a hole size distribution plot normalized for comparison with Figure 3, the particle size distribution as described in Reference 3. There is a departure from proportionality below about 100 μ perforation.

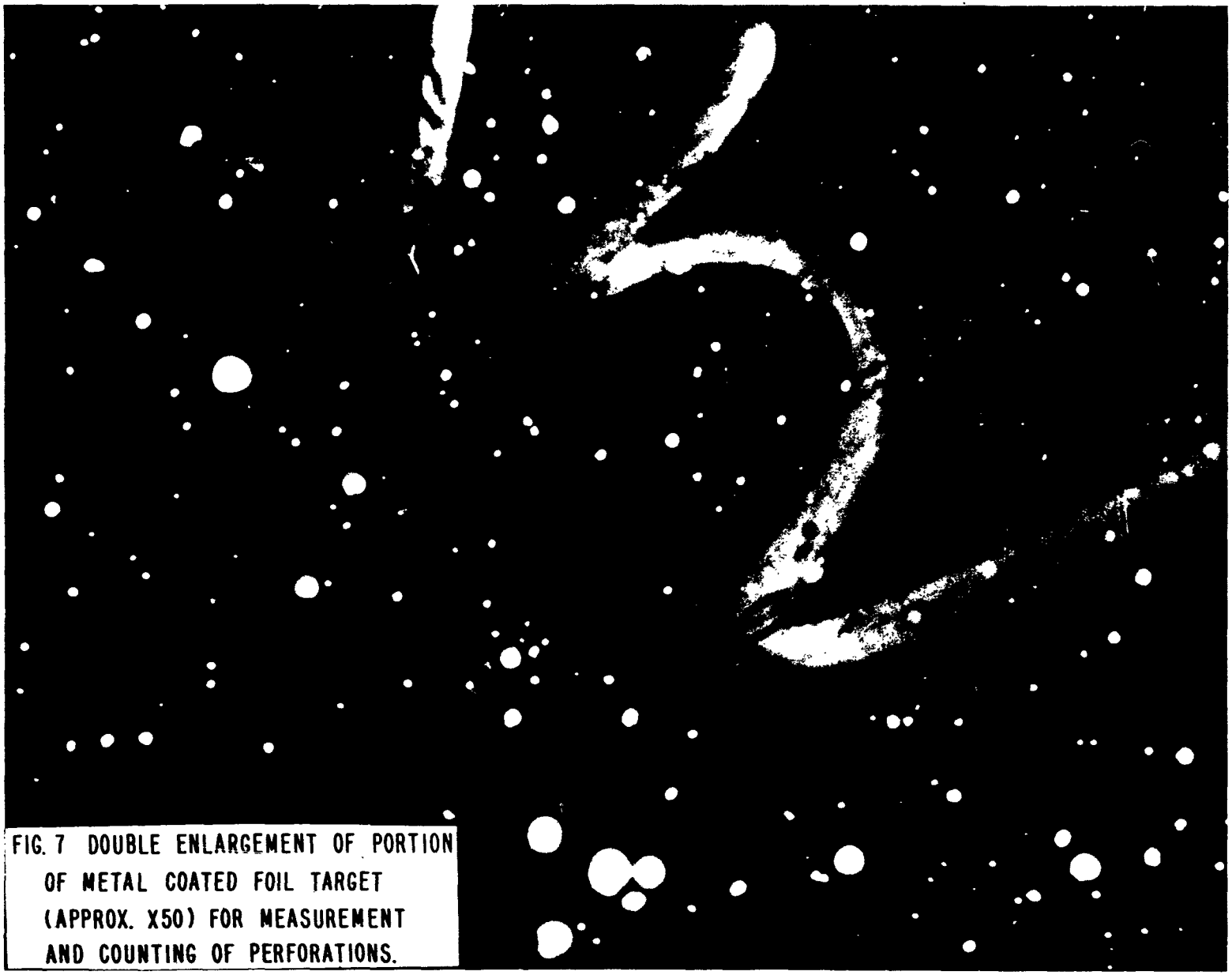

FIG. 7 DOUBLE ENLARGEMENT OF PORTION OF METAL COATED FOIL TARGET (APPROX. X50) FOR MEASUREMENT AND COUNTING OF PERFORATIONS.

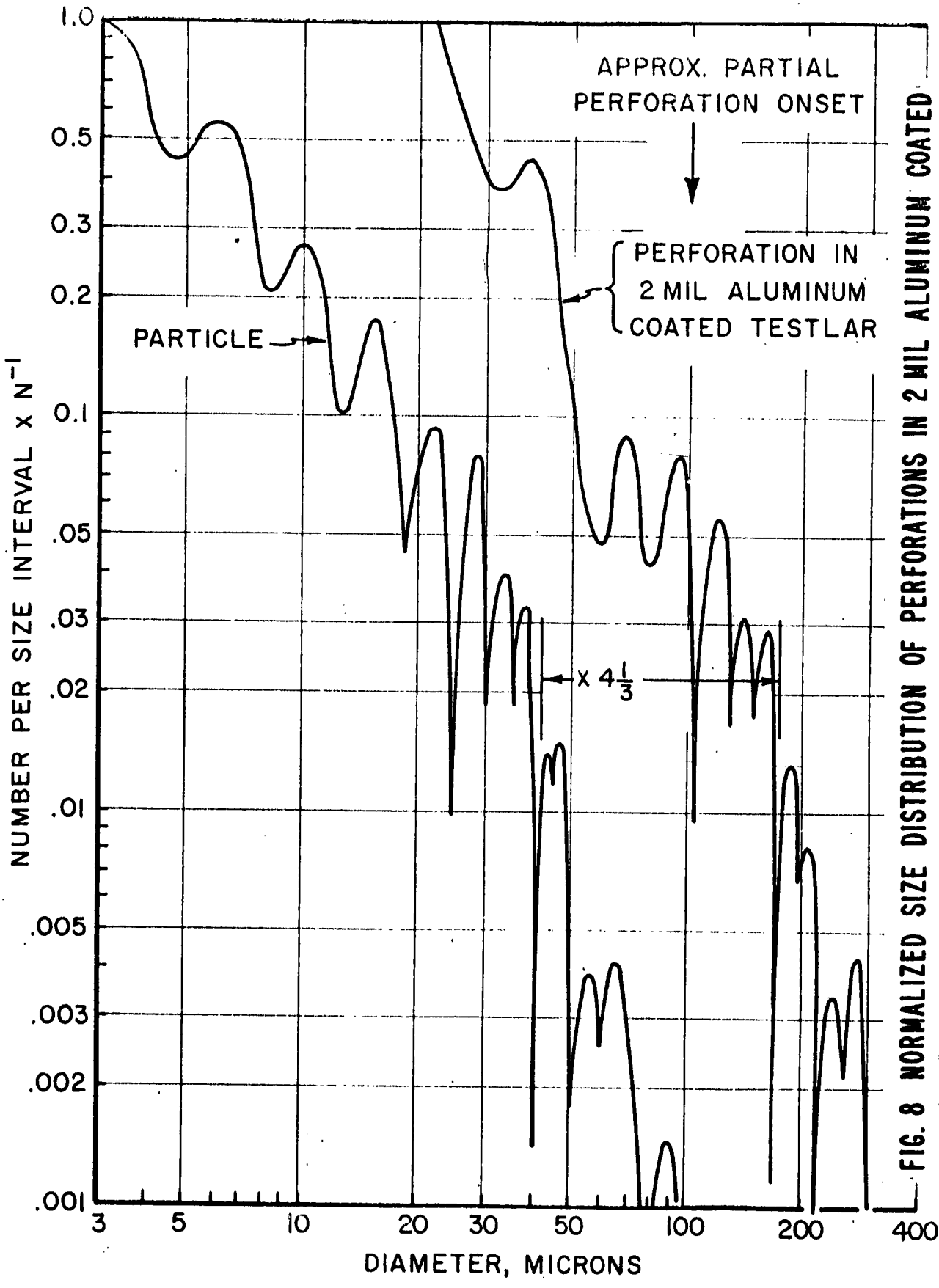

FIG. 8 NORMALIZED SIZE DISTRIBUTION OF PERFORATIONS IN 2 MIL ALUMINUM COATED TESTLAR TARGET COMPARED TO SIZE DISTRIBUTION OF RESPONSIBLE PARTICLES

Considering the hemispherical shape of hypervelocity craters in semi-infinite targets (Reference 3), and the condition that this is a 2-mil thick foil specimen, it can be interpreted that a transition of mechanism would be expected in the vicinity of 100μ crater diameter or 50μ depth. This transition from perforation to pseudo-infinite cratering has been reported merely as onset of partial perforation, with no attempt to separate the ballistic limit phenomena such as spalling, punching out, imbedding etc. Simple detection of the transition suffices for evaluation of reduction in strength and reflectivity of the foil. However, in this connection it should be mentioned that the results reported here are based on measurements of apparent optical diameter of the perforations. No correction for the optical properties of these translucent materials has been attempted.

As shown in Figure 4, there is a disturbed area surrounding each impact point in Mylar. On the other hand, in uncoated Testlar targets, the impacts were not optically detectable. This would suggest that the refractive index of Testlar does not differ greatly from that of air. Further, since the profiles of the perforations are still invisible after impact, any change in the optical properties which may occur must be annealed out by conversion of some impact energy to local heating. In contrast Mylar does differ in optical values from the surrounding air; also, under impact, it absorbs some of the available energy in plastic deformation and stores a portion as mechanical strains in the material.

Figure 9 indicates some of the probable anomalies of the apparent optical diameter in thin foil hypervelocity impact. The upper figure represents the condition of definite complete perforation. D_c indicates the diameter of the hole at the original surface. However, one has no assurance that this is what is seen either microscopically or by comparator, nor whether it is what the photographic enlarger shows. Depending on the optical properties of the drastically disturbed material around the perforation, one may be observing $D_{(-)}$. $D_{(-)}$ is the minimum opening, including any contribution of the curvature of the wall of the hemispherical

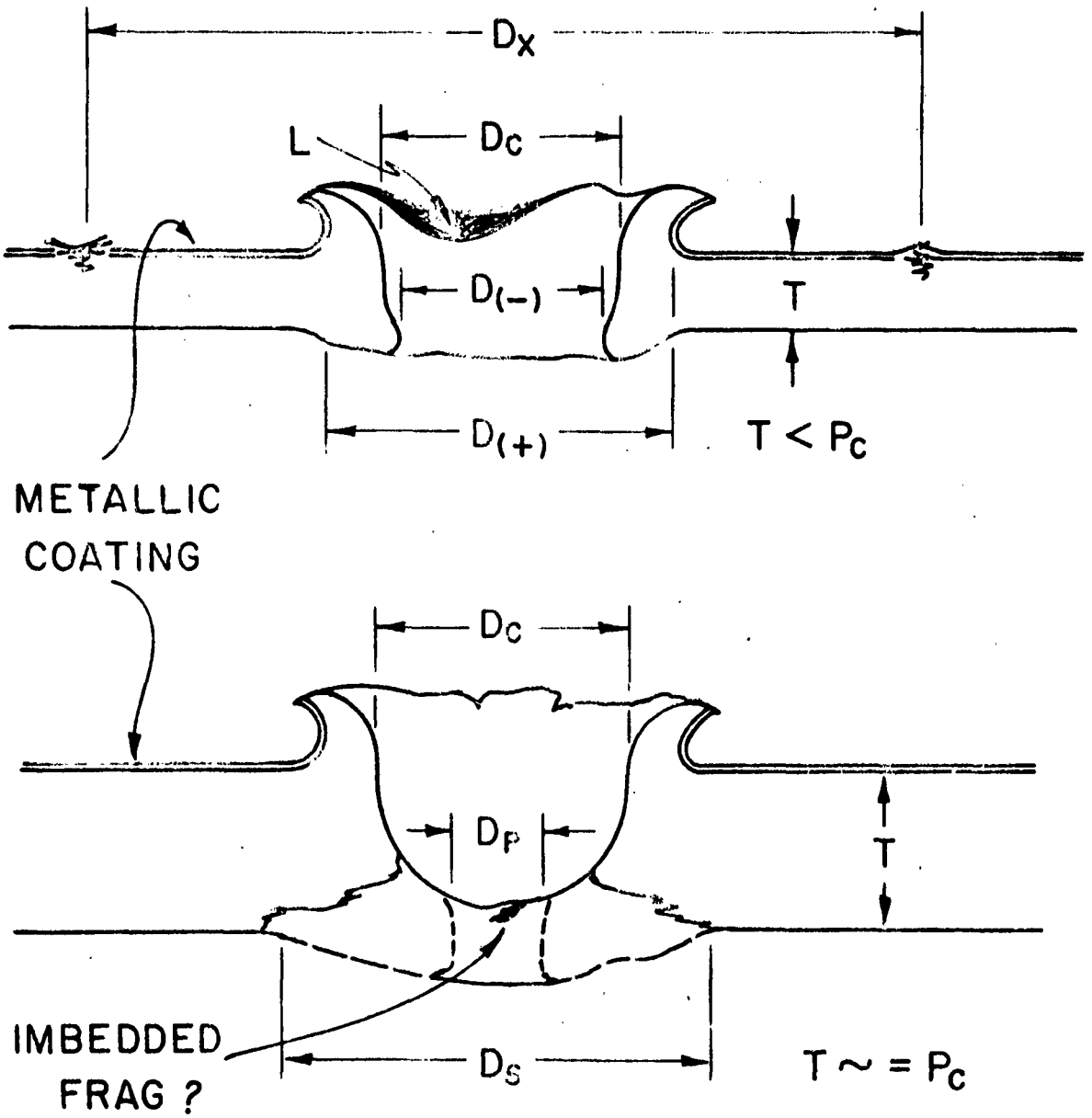

FIG. 9 SKETCH OF TYPICAL HYPERVELOCITY IMPACTS ON THIN TRANSLUCENT FOILS INDICATING PROBABLE CAUSES OF OPTICAL ANOMALIES

hypervelocity crater and the elastic or plastic recovery, and also including the possible doubling inward of portions of the crater petal, L. On the other hand one may be observing $D_{(+)}$, the minimum opening between the folded back metallic coating on the foil, further influenced by the optical properties of the disturbed material in the crater wall.

Some materials exhibit the phenomenon labled D_x around the larger perforations (Figure 5). This consists of a broken, but more or less complete circle of translucent smears, spaced from the crater at about the distance that the original surface is raised in a semi-infinite ductile target. This ring probably represents some local failure of the metallic coating bonding due to some mismatch of yield point properties between that metallic coating and the foil beneath.

Considering the case of something less than complete perforation, the lower half of Figure 9 indicates that the observed diameter could be either D_p, the diameter of the punched out plug; D_s, the diameter of the minimum hole with the effects of spall, or in the instance of no perforation, only the diameter corresponding to $D_{(+)}$ above. Some spots on the prints exhibit a darker shadow in the center, which could be an imbedded fragment. Others show the central shadow spread into a ring, as would be expected from the optical effects of a minute, punched plug. Some alternate technique of confirming the optical observations is desirable, not only to determine which of these apparent diameters is being measured in a specific target material, but also to provide a means of analyzing the uncoated Testlar foils.

None of the optical anomalies described would be significant for the application of this method to simple metal foils, where only the minimum opening $D_{(-)}$ will be observed because of their uniform opacity. Figure 10 shows an enlarged print of a 2-mil Al target and Figure 11 similarly represents a specimen of 2-mil Pb.

As shown in Table I under the column marked "D_c/D_p Ratio", the ratios of crater diameter to pellet diameter fall into two groups. One group includes all the stainless steel coated materials in both thicknesses as

FIG. 10 PHOTOGRAPHIC ENLARGEMENT OF 2 MIL ALUMINUM FOIL TARGET (APPROX. X 9)

FIG. 11 PHOTOGRAPHIC ENLARGEMENT OF 2 MIL LEAD FOIL TARGET (APPROX X 9)

well as the "Aluminized" 0.5-mil Mylar. The values in this group range from 2.8 to 3. The other group, with a range from 4 to 4.8, includes the aluminum coated materials in both thicknesses and the uncoated 2-mil Mylar. This indicates that one major influence on the final values is the nature of the metallic coating, probably appearing by way of the effect on the dimensions shown in Figure 9 as $D_{(+)}$. For a particular type of metallic coating, the optical properties of the base foil provide a contribution of the order of 15%, while, between differing types of metallic coatings, the values differ as much as plus or minus 20%. For a particular foil material the comparison of corresponding frequency maxima and minima shows a variation of about 10%, and this being the estimated accuracy of tests on a specific material.

III. RESULTS

A. Tabulated Experimental Results:

The results of the impact exposure analysis are summarized in Table I of the Appendix. More detailed listings of the impact intensities sustained by individual target specimens of the various materials are further expanded in Tables II thru XI of the Appendix.

The first four columns of Table I identify the target material. Column 5 reports a numerical ratio of perforation diameter to corresponding particle diameter, obtained as indicated in Figure 8. This designation, D_c/D_p, is retained from the similar application to semi-infinite targets. (Reference 3) However, the D_c values used in this work are apparent diameters of the perforations, which probably include some contribution from the optical properties of the Mylar and Testlar foil material as explained above.

A comparison of individual pairs of maxima and minima from the two size distributions results in a range of D_c/D_p ratios differing by 10%. This is caused by the arbitrary choice of the limits of the statistical intervals used in summing the distributions and indicates the influence on overall accuracy which such interval choice exerts on distributions where the frequency maxima and minima are very sharp.

Column 6 indicates the particle size below which the respective size distributions depart from proportionality. Referring to the arrow at 100μ on Figure 8, this value corresponds to a hole diameter (and depth) such that the target begins to react as a semi-infinite one. Therefore, this value is reported as the onset of a "Partial Perforation Transition".

Column 7 reports a coded expression as per NOTE 3 for the approximate impact exposure intensity. This value is a very rough estimate of the total number of impacts sustained. The individual materials are reported in more detail in Tables II to XI. Values for columns 5 and 6 of Table I were determined from the totals of all target specimens of a particular type and therefore pertain to that specific material.

B. Incidential Results:

1. In order to provide an estimate of the target damage due to elements of the apparatus other than the microparticles, representative specimens were subjected to such incidental effects as shock and blast without projected particles. In one arrangement, the apparatus was assembled and fired in the same manner as a regular test but without a liner in the projection charge to fragment into particles. The other arrangement utilized the explosive shuttering device alone with no projection charge. In both cases the target specimens exhibited no perforations.

2. When it became evident that many of the projected particles more than about twenty microns in size were perforating with energy to spare the possibility of damage to an inflated space vehicle during the exit phase out the far side of the balloon was considered. Since such particles in striking from the inside would impact the uncoated side of the foil material, a test was made of a coated specimen with the uncoated side exposed to the impacts. The metallic coating peeled back from the perforations in a ragged manner indicating that the wrong side impacts do not produce the same result as impacts on the coated surface. However, as the perforations did not exhibit simple circular profiles, analysis by statistical measurement as described above was not possible.

3. Mylar foils of 0.5-mil thickness, particularly in the uncoated and the "aluminized" condition were found to be subject to a tendency to tear under the stresses of the test exposure. This difficulty was not experienced with Testlar or with the 2-mil thickness in the Mylar.

4. In the uncoated condition, Mylar (Figure 4) exhibited markedly reduced transparency surrounding the impacted regions, while uncoated Testlar was not sufficiently disturbed in its optical properties to permit exposure analysis by optical methods.

5. In some instances aluminum coatings exhibited a slight tendency to discolor under intense impact. This was not observed with stainless steel coatings. Similar discoloration has been observed in semi-infinite

copper subjected to hypervelocity impact. This discoloration has been approximated by surface oxidation tests at a few hundred degrees centigrade. In the semi-infinite target the body of the specimen acts as a heat sink for dissipation of this energy from the immediate vicinity of the point of impact. A thin foil effectively reduces the available heat sink from three dimensions to two. Thus discoloration resembling oxidation on thin foil targets under hypervelocity impact indicates that some of the energy of the impacting particle is absorbed and converted into heat.

6. Myler foil 0.5-mils thick in the uncoated condition tended to scorch and shrivel under moderately intense impact in spite of the vacuum environment.

IV. CONCLUSIONS

1. Coated and Uncoated foil specimens, subjected to micro-particle impact at velocities of 12 Km/sec. showed a relationship of perforation size to impacting particle size ranging between 2.8 and 4.3 depending on the particular foil tested (See Appendix Table I).

2. A departure from agreement between the particle size and perforation size frequency distributions was observed in the vicinity of perforation diameter approximately twice the foil thickness. The corresponding particle size for a given velocity in this critical region determines whether or not perforation is accomplished. Therefore this value is reported as the onset of a transition between mechanisms of perforation and cratering.

3. Steel coated foils in either Mylar or Testlar always gave a lower D_c/D_p ratio than aluminum coated or bare foils.

4. No significant differences were observed between Testlar and Mylar foils when compared under similar coating conditions, although Mylar did show some tendency to tear and scorch in areas of intense exposure whereas Testlar did not.

L. G. RICHARDS

J. W. GEHRING, JR.

V. A P P E N D I X

TABLE I

MATERIAL	THICKNESS (MILS)	COATING	CODE DESIG.	D_c/D_p RATIO (Note 1)	PARTIAL PERFORATION TRANSITION (Note 2)	EXPOSURE (Note 3)	EXPOSURE DETAIL	NOTES AND REMARKS
Mylar	0.5	Bare	M5B					Scorched and Burned.
Mylar	2.0	Bare	M2B	4-1/3	22 Microns	FH - FG	Table II	Discolored under intense exposure
Mylar	0.5	Steel	M5S	2.8	8 Microns	FH - SH	Table III	Tore under intense exposure
Mylar	2.0	Steel	M2S	3.	30 Microns	FH	Table IV	
Mylar	0.5	"Aluminized"	(Note 4)	3.	9 Microns	SG	Table V	Tore under intense exposure
Mylar	0.5	Aluminum	M5A	4.4	6 Microns	FH - MG	Table VI	
Mylar	2.0	Aluminum	M2A	4.	25 Microns	SH - FG	Table VII	
Testlar	0.5	Bare	T5B					Note 5
Testlar	2.0	Bare	T2B					Note 5
Testlar	0.5	Steel	T5S	2.9	9 Microns	FG	Table VIII	
Testlar	2.0	Steel	T2S	3.	18 Microns	estimate (Note 6)	Table IX	Coating poorly bonded.
Testlar	0.5	Aluminum	T5A	4.8	3 Microns	FH - FG	Table X	
Testlar	2.0	Aluminum	T2A	4-1/3	20 Microns	SG - MG	Table XI	Discolored, probably oxidized

NOTES TO TABLE I

NOTE 1. Ratio of apparent optical diameter of perforation to the equivalent diameter of responsible particle treated as sphere.

NOTE 2. Particle size at which the perforation size distribution departs from the particle size distribution proportionality, ascribed to the transition in mechanism associated with the beginning of incomplete perforation.

NOTE 3. Impact exposure intensity coded as follows:

SYMBOL	NUMBER OF IMPACTS
FH	Few hundred
SH	Several hundred
FG	Few thousand
SG	Several thousand
MG	Many thousand

NOTE 4. Early work was performed in testing half-mil "aluminized" Mylar before the material with the continuous aluminum coating (M5A) became available. The "aluminized" coating, applied by a different technique, was observed to behave differently, the resulting material being more susceptible to mechanical damage incidental to testing than was the "aluminum coated" Mylar tested later.

NOTE 5. The optical qualities of uncoated TESTLAR were found to be of such a nature that the impacts were not optically discernable for analysis.

NOTE 6. Stainless steel-coated TESTLAR of 2-mil thickness exhibited very poor bonding of the coating of such an extent that relatively large areas of the exposed portion could not be brought into sharp common focus. As it was felt that the poor quality of this material would require improved fabrication before use in inflatable space structures would be justified, values reported were estimated without thorough analysis.

TABLE II

Material - Mylar* Partial Perforation Transition 22 Microns

Thickness - 2 Mil D_c/D_p - 4-1/3

TARGET M2B-8

Perf.Size (Microns)	Number obs
44	1
38	2
27	2
22	4
10	60
3 est	400

TARGET M2B-9

Perf.Size (Microns)	Number obs
61	2
49	10
37	33
28	45
21	210
12 est	1000
3 est	4700

*Illustrated in Figure 4

TABLE III

Material - Mylar — Partial Perforation Transition 8 Microns

Thickness - 0.5 Mil — D_c/D_p - 2.8

Coating - Stainless Steel

TARGET M5S-13

Perf. Size (microns)	Number obs.
60	1
45	2
36	2
28	1
21	4
10	55
3 est	138

TARGET M5S-14

Perf. Size (Microns)	Number obs.
45	1
28	2
22	4
10	33
3	100

TARGET M5S-15 estimated (specimen tore under test impact)

Perf Size (Micron)	Number obs.
65	2
44	5
37	8
27	10
22	23
10	300
3	1000

TABLE IV

Material - Mylar — Partial Perforation Transition 30 Microns

Thickness - 2 Mils — D_c/D_p - 3

Coating - Stainless Steel

TARGET M2S-20

Perf. Size (Microns)	Number obs.
43	1
33	2
27	4
21	35
10	50
3	200

TARGET M2S-21

Perf. Size (Microns)	Number Obs
68	5
43	1
36	2
25	9
20	30
10	80
3	300

TABLE V

Material - Mylar — Partial Perforation Transition 9 Microns

Thickness - 0.5 Mil — D_c/D_p - 3

Coating - "Aluminized"*

TARGET No. 379

Perf. Size (Microns)	Number Obs
51	6
45	17
38	37
27	500
23	550
10	1400
3	5000

*The "Aluminized" coating on this material was not applied in the same manner as that on the aluminum coated inflatable structure materials. However, this material was used for early tests to develop the method.

TABLE VI

Material - Mylar — Partial Perforation Transition 6 Microns

Thickness - 0.5 Mil — D_c/D_p - 4.4

Coating - Aluminum

TARGET M5A-31

Perf. Size (Microns)	Number obs.
56	1
47-48	3
43	7
36	26
31	21
28	23
24	20
18	65
14-15	125
10-11	250
6-7	450
3	600

TABLE VI

TARGET M5A-32

Perf. Size (Microns)	Number obs.
56	1
47-48	1
43	2
36	2
31	1
28	2
24	1
18	8
14-15	14
10-11	30
6-7	75
3	100

TABLE VI

TARGET M5A-33

Perf. Size (Microns)	Number obs.
56	1
47-48	4
43	8
36	22
31	19
28	24
24	22
18	100
14-15	225
10-11	700
6-7	2700
3	3400

TABLE VII

Material - MYLAR

Thickness - 2 Mil

Partial Perforation Transition 25 Microns

D_c/D_p - 4

TARGET M2A-37

Perf. Size (Micron)	Number obs.
65	5
55	2
48	2
43	5
37	9
31	4
26	4
21	20
14-18	100
10-11	320
6-7	800
3	1000

TARGET M2A-38

Perf. Size (Microns)	Number obs.
65	1
48	1
37	1
31	2
26	2
21	4
14-18	30
10-11	100
6-7	300
3	400

TARGET M2A-39

Perf. Size (Microns)	Number Obs.
65	1
55	1
48	1
43	2
31	2
26	2
21	8
14-18	50
10-11	170
6-7	500
3	613

TABLE VIII

Material - Testlar — Partial Perforation Transition 9 Microns

Thickness - 0.5 Mil — D_c/D_p - 2.9

Coating - Stainless Steel

Specimen T5S-13 Very few hits, insufficient for analysis. Estimate

TARGET T5S-13

Perf. Size (Microns)	Number obs.
over 25	2
20-25	4
10-20	35
less than 10	100

TARGET T5S-14

Perf. Size (Microns)	Number obs.
50	2
38	10
28	17
20	45
10	900
2	3000

TABLE IX

Material - Testlar

Thickness - 2 Mil

Coating - Stainless Steel

Failure of the bond between the Testlar base and the Stainless Steel Coating prevented thorough analysis of this material. Use in an inflatable satellite would require rectification of this shortcoming. Exposure of T2S-23 is estimated.

TARGET T2S-23

Perf. Size (Microns)	Number obs.
38	4
27	44
22	400
11	700
3	2000

A D_c/D_p ratio of 3, was used as a partial guide in arriving at the above estimated exposure.

TABLE X

Material - Testlar — Partial Perforation Transition 3-4 Microns

Thickness - 0.5 Mil — D_c/D_p - 4.8

Coating - Aluminum

TARGET T5A-31

Perf. Size (Microns)	Number obs.
38	1
28	2
18	8
14-15	15
10-11	20
61-7	80
3	100

TARGET T5A-32

Perf. SSize (Micron)	Number obs.
65	8
44	4
38	7
34	11
28	21
24	51
18	75
14-15	193
10-11	400
6-7	1000
3	1300

TABLE XI

Material - Testlar — Partial Perforation Transition 20 Microns

Thickness - 2 Mils — D_c/D_p - 4-1/3

Coating - Aluminum

Specimen T2A-25 was large enough to provide two test targets.

Perf. Size (Microns)	No. 402	No. 403
61	2	2
50	5	10
36	7	10
27	10	15
22	30	45
10	900	1200
3	4000	5000

TARGET T2A-26

Perf. Size (Microns)	Number obs.
75	1
64	5
43	33
37	34
27	48
22	125
9	4000
3	30000

The phenomena of Figure 9 marked D_x and L are particularly prevalent in this material.

The very intense exposure of specimen T2A-26 resulted in discoloration of the Aluminum coating, probably local oxidation. Figure 5 illustrates this material

VI. REFERENCES

1. Kineke, J. H. and Gehring, J. W. "Preliminary Investigations of Simulated Micro Meteorite Impact", BRL Tech Note No. 1134, July 1957; and, Kineke, J. H. and Holloway, L. S. "Macro-Pellet Projection With an Air Cavity High Explosive Charge for Impact Studies", BRL Tech Note No. 1264, April 1960.

2. "Proceedings of Third Symposium on Hypervelocity Impact", Chicago 1958, Armour Research Foundation, 1959; and, "Proceedings of Fourth Symposium on Hypervelocity Impact", Eglin Air Force Base, April 26-28, 1960, Air Proving Ground Center 1960, Papers by Gehring, Kineke and Feldman.

3. Richards, L. G. and Holloway, L. S. "Study of Hypervelocity Micro-Particle Cratering", BRL Memo Report No. 1286, June 1960.

4. Leonard, R. W., Brooks, G. W. and McComb, H. G. "Structural Considerations of Inflatable Re-entry Vehicles", NASA Tech Note No. D-457, September 1960; and, "Sky and Telescope", February 1960, pp. 220-204 and 222-223.

DISTRIBUTION LIST

No. of Copies	Organization
2	Chief of Ordnance ATTN: ORDTB-Bal Sec ORDTU Department of the Army Washington 25, D. C.
1	Commanding Officer Diamond Ordnance Fuze Laboratories ATTN: Technical Information Office, Branch 012 Washington 25, D. C.
2	Director Naval Research Laboratory ATTN: Technical Information Division Mr. Walter Atkins Washington 25, D. C.
2	Commanding General Army Ballistic Missile Agency ATTN: Henry Martin John Heamon Redstone Arsenal, Alabama
1	Commanding General Army Rocket and Guided Missile Agency ATTN: Technical Library, ORDXR-OTL Redstone Arsenal, Alabama
2	Director Advanced Research Projects Agency ATTN: Col. R. Wilder Department of Defense Washington 25, D. C.
1	Director National Aeronautics and Space Administration Ames Research Center ATTN: Dr. A. C. Charters Moffett Field, California
1	Director National Aeronautics and Space Administration Langley Research Center ATTN: Mr. Robert W. Leonard Langley Field, Virginia
1	Director IDA/Weapon Systems Evaluation Group Room 1E880, The Pentagon Washington 25, D. C.
1	Chief of Research & Development ATTN: Lt. Col. J. T. Brown, Army Research Office Department of the Army Washington 25, D. C.
12	General Electric Company MSVD 3198 Chestnut Street Philadelphia 4, Pennsylvania
1	Carnegie Institute of Technology Department of Physics ATTN: Prof. Emerson M. Pugh Pittsburgh 13, Pennsylvania

UNCLASSIFIED